NESC Webinar, November 16, 2023

Combustion of Metal Powders for Power and Heat Generation in Space Missions

Evgeny Shafirovich

Department of Aerospace and Mechanical Engineering

The University of Texas at El Paso

eshafirovich2@utep.edu

Acknowledgments

NASA Space Technology Research Grants Program

- Early Stage Innovations Grant #80NSSC20K0293
- January 13, 2020 – January 12, 2023
- NASA Collaborator: **Steven Rickman**, NESC
- Collaborators for combustion modeling (not included in this presentation): Prof. **Vladimir Volpert** and Prof. **Alvin Bayliss**, Northwestern University

Graduate Students

- **Sergio Cordova**, PhD from UTEP, currently at Northrop Grumman
- **Kevin Estala-Rodriguez**, PhD from UTEP, currently at the DOE Office of Environmental Management

Space Power Systems

Vertical solar array on the Moon (under development)

Radioisotope thermoelectric generator (RTG) of Curiosity rover

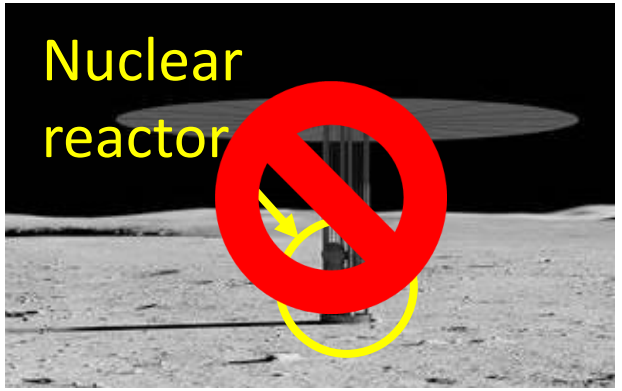

Conceptual nuclear power system on the Moon

Lithium-ion batteries for Sojourner rover

Combustion-based power system

- Specific energy and power are higher than for batteries.
- Unlimited energy storage time
- Especially advantageous if the lander or rover needs to be heated.

Image credits: NASA and JPL

Power System Based on Li-SF_6 Combustion

Li-SF_6 combustion has been used in the U.S. Navy's Mk-50 torpedoes.

- $8Li + SF_6 \rightarrow 6LiF + Li_2S$ 14.1 MJ/kg
- The condensed products occupy less volume than the used lithium.

Mk-50 torpedo being fired
Credit: U.S. Navy

Was recently under development at JPL for lunar night survival.

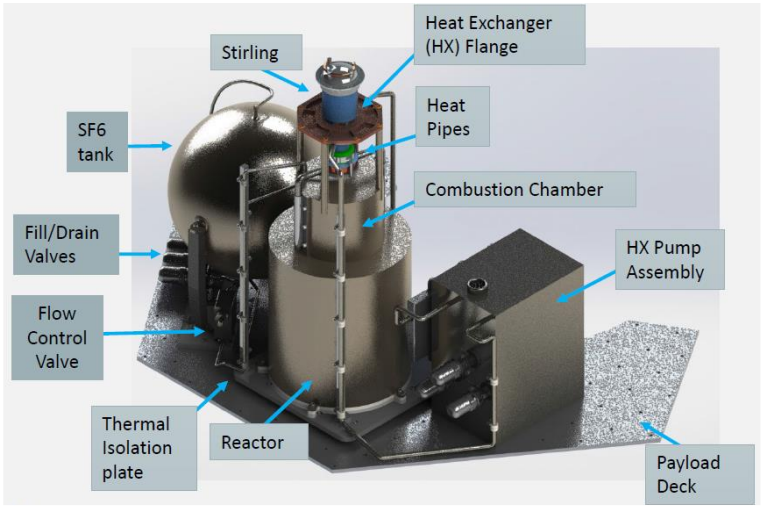

Li-SF_6 power system for lunar night survival

Reactor

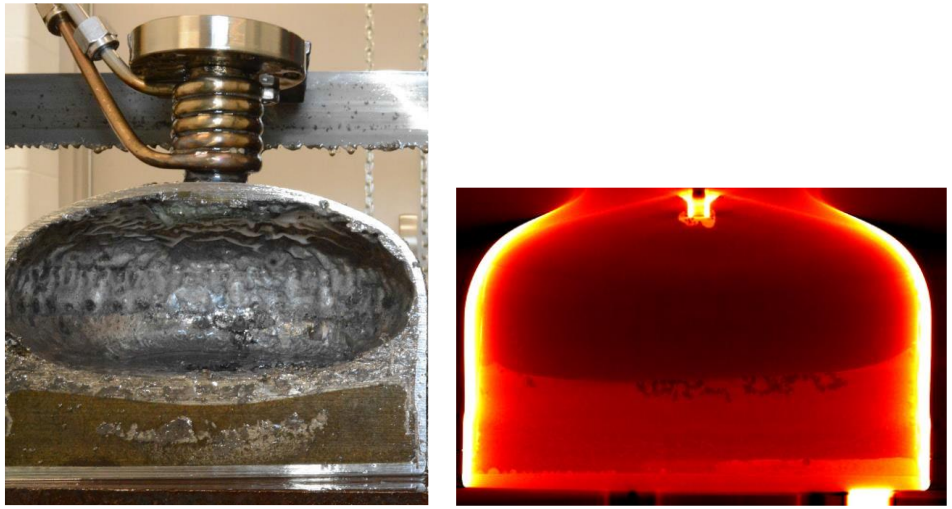

Cross-sectioning and CT scan of the reactor

M. Hunter et al., "Heat and electrical power for surviving the lunar night: the chemical heat integrated power source (CHIPS)," 2022 Conference on Advanced Power Systems for Deep Space Exploration

Power System Based on Li-CO_2 Combustion

Was studied at Penn State – Applied Research Laboratory for cooling a Venus lander.

- Venus surface: 92 bar, 470 – 500 °C
- Li-CO_2 batch reactor combustion experiments

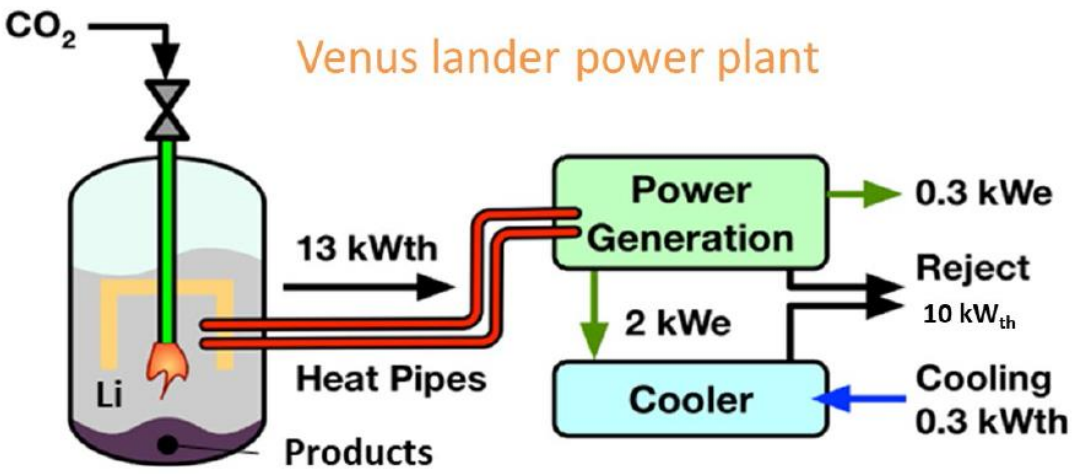

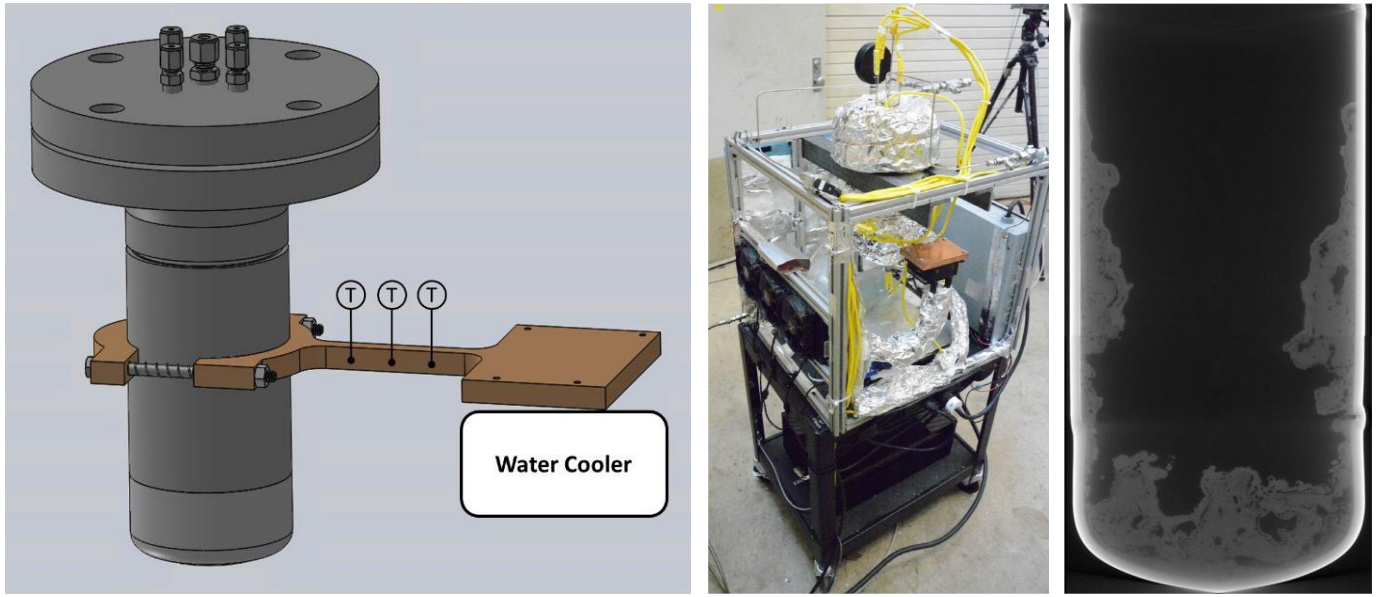

Schematic, photo, and CT scan of the reactor

C.J. Greer et al., "Metal fueled, chemical heat and power sources and conversion cycles for extreme environment planetary landers," 2022 Conference on Advanced Power Systems for Deep Space Exploration

Metal – O_2 Combustion?

Energy per kilogram of the reactants

$2Be + O_2 \rightarrow 2BeO$	24.3 MJ/kg
$4Li + O_2 \rightarrow 2Li_2O$	20.0 MJ/kg
$4Al + 3O_2 \rightarrow 2Al_2O_3$	16.4 MJ/kg
$2Mg + O_2 \rightarrow 2MgO$	14.9 MJ/kg

$8Li + SF_6 \rightarrow 6LiF + Li_2S$ 14.1 MJ/kg

Chemical oxygen generator ("oxygen candle")

- Oxygen source: chlorates and perchlorates of Li or Na
- Widely used in aircraft, submarines, and space stations

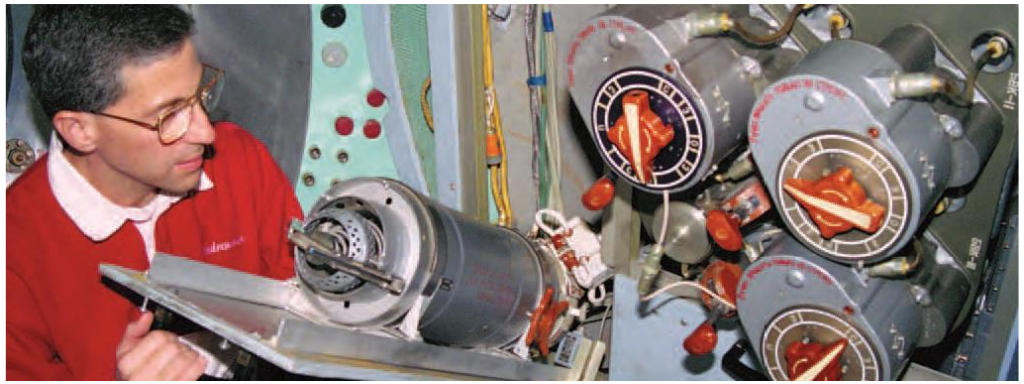

A chemical oxygen generator for space stations

Image credit: NASA

Metal-O_2 Power System

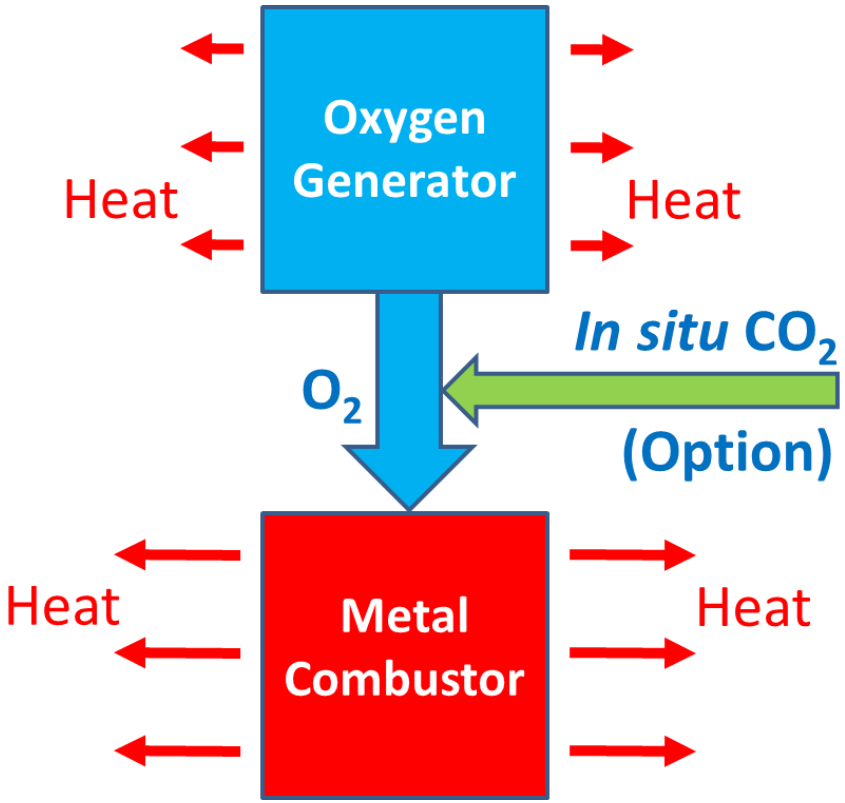

- The generated oxygen infiltrates through the metal powder to the reaction zone.
- Combustion is controlled by oxygen flow.
- Solid reactants and products
- Unlimited storage time
- Optional use of *in situ* CO_2 (Mars and Venus)

“Filtration Combustion” of Metal Powders

- Used for combustion synthesis of metal nitrides and hydrides.
  - Pressures over 1000 bar in the reactor to ensure enough gas in the reaction zone
- In space power systems, pressure must be much lower.
- Infiltration of the gaseous oxidizer due to pressure gradient is critical.

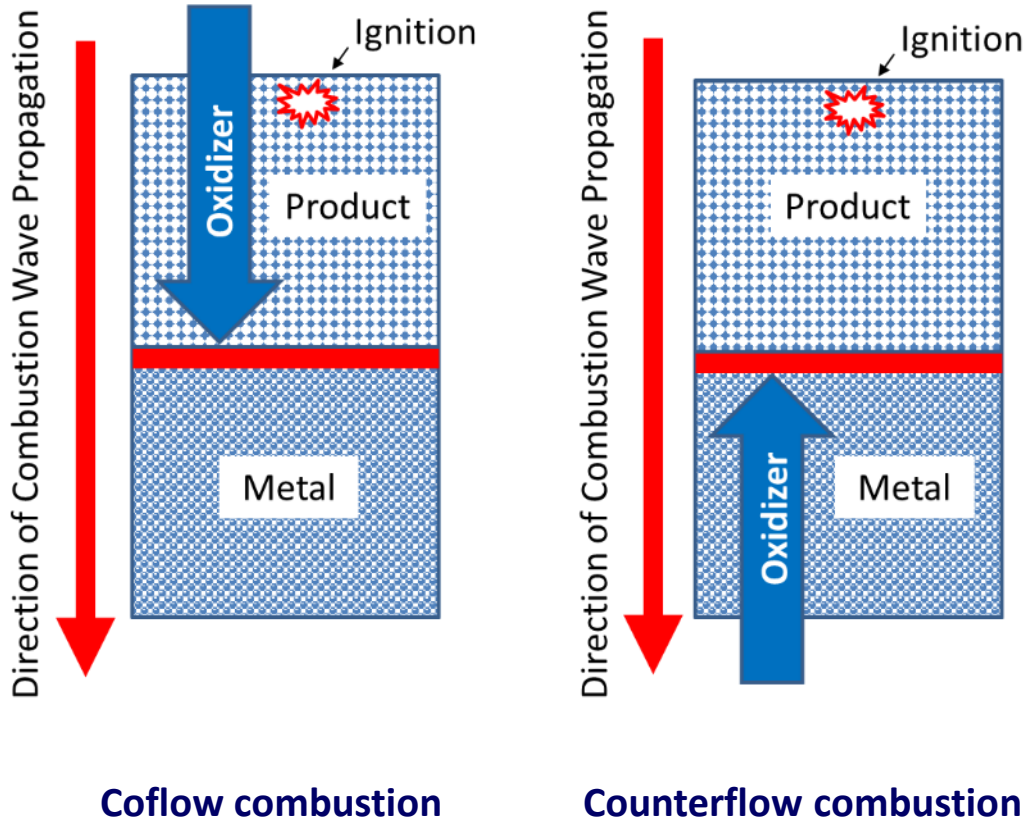

Selection of Metal Fuel

Pilling-Bedworth ratio: $R_{PB} = \frac{Product\ volume}{Metal\ volume}$ **R_{PB} < 1 is desired.**

R_{PB} = 1.70

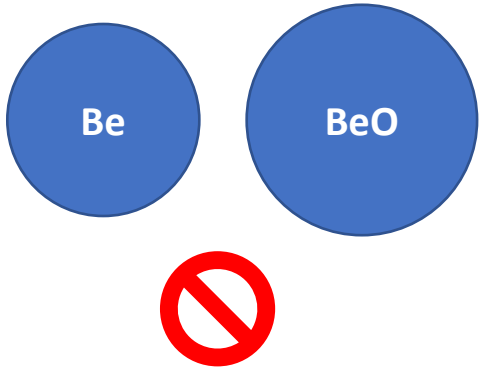

R_{PB} = 1.28

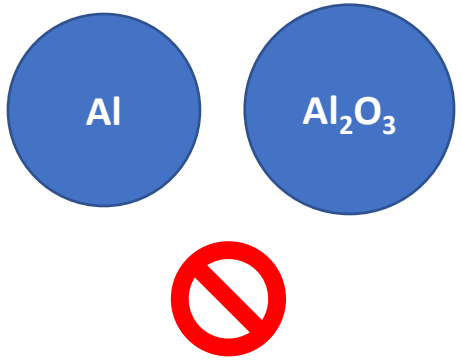

R_{PB} = 0.81

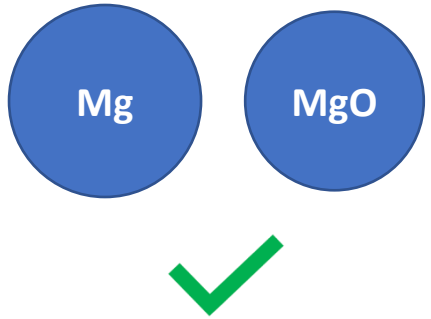

R_{PB} = 0.57

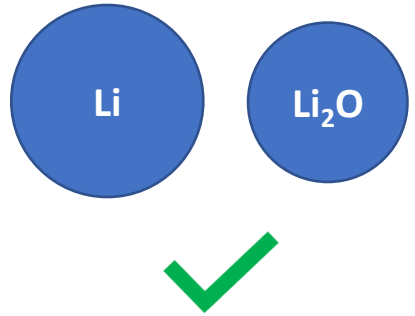

Li and Mg have been selected for further studies.

Mass Estimates for Lunar Night Survival

Li – SF_6 (JPL design)

SF_6 tank

- 15.84 kg, including 11.94 kg SF_6 (liquid at 22 bar and 294 K)

Mass of metal fuel

- 4.58 kg Li

Heat release

- 157 MJ

$$\frac{157}{15.84 + 4.58} = 7.7\ \frac{MJ}{kg}$$

Metal – oxygen generator

Multi-purpose oxygen generator (MPOG, Molecular Products, 2600 L of O_2 at NPT)

- 12 kg, including 3.46 kg of oxygen

Mass of metal fuel

- 3.00 kg Li or 5.25 kg Mg

Heat release

- 132 MJ

Li:
$$\frac{132}{12 + 3.00} = 8.8\ \frac{MJ}{kg}$$

Mg:
$$\frac{132}{12 + 5.25} = 7.7\ \frac{MJ}{kg}$$

Note: Mg is 3.25 times denser than Li.

MPOG

Credit: Molecular Products

T.J. Hendricks et al., "Chemical heat integrated power source (CHIPS) to survive the lunar night environments," 2020 Conference on Advanced Power Systems for Deep Space Exploration

Multiple Heat-generating Cartridges

Could be used in a long mission, such as the lunar night survival.

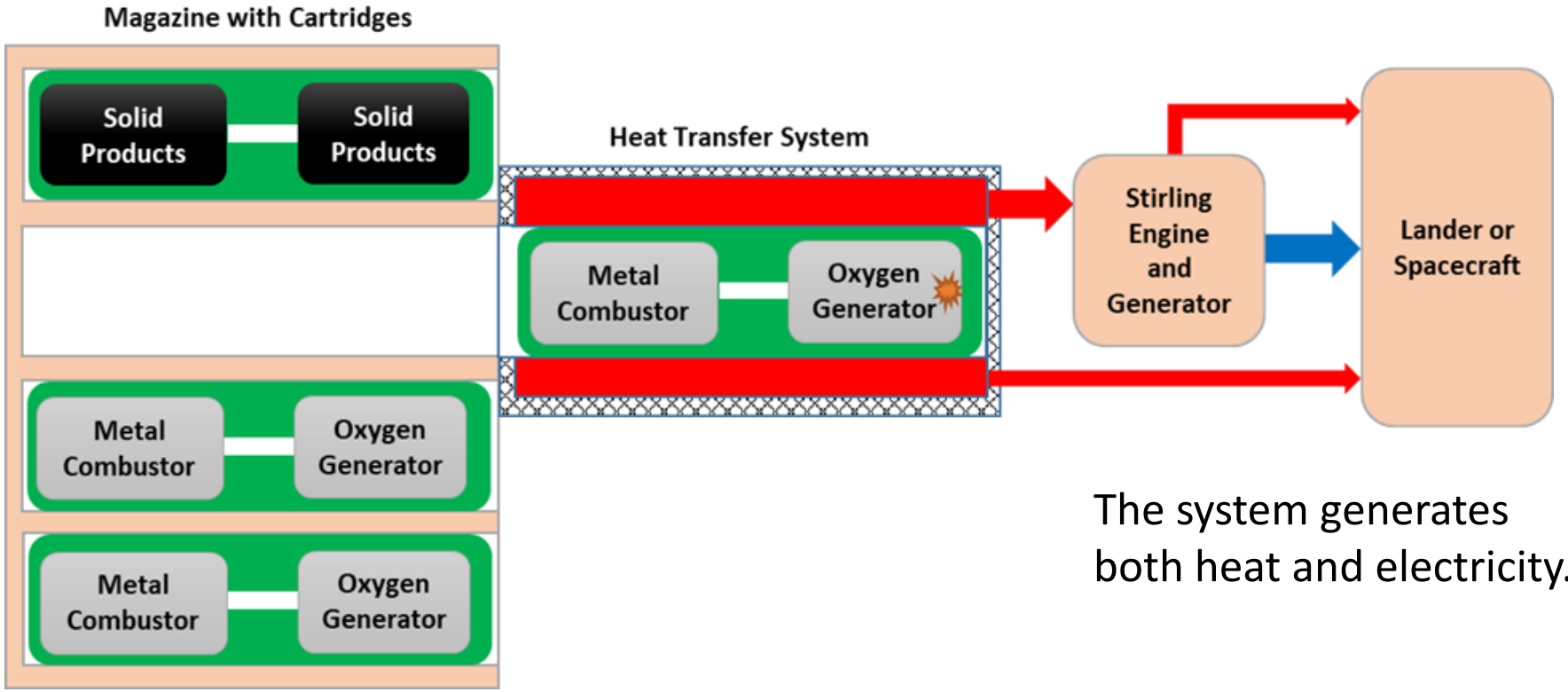

The system generates both heat and electricity.

Power system with cartridges

E. Shafirovich, "Conceptual design of a space power system based on combustion of metals," *Journal of Propulsion and Power* 39 (2023) 464-468

Mass Estimates for Design with Cartridges

Lunar night survival mission, 14 days, total energy: 157 MJ (44 kWh)

- Li – SF_6 (JPL design)
- Li – COGs for aircraft
- Mg – COGs for aircraft

COGs for aircraft

Credit: B/E Aerospace

	Li – SF_6	Li - COGs	Mg - COGs
Mass of SF_6 tank, kg	**15.84**	-	-
O_2 capacity of COG, L	-	80	80
Mass of COG, kg	-	0.45	0.45
Number of cartridges	-	40	40
Mass of all COGs, kg	-	**18**	**18**
Mass of fuel, kg	**4.58**	**3.69**	**6.46**

The masses of all COGs and Li or Mg are comparable with those of SF_6 tank and Li.

E. Shafirovich, "Conceptual design of a space power system based on combustion of metals," *Journal of Propulsion and Power* 39 (2023) 464-468

Research Objectives

1. **Kinetics and mechanisms of Mg and Li reactions with O_2 and CO_2**
   - Thermoanalytical methods (TGA and DSC)

2. **Combustion of Mg and Li powders with infiltrating O_2 and CO_2**
   - Closed chamber; pressure difference due to consumption of the oxidizer → natural infiltration
   - If the combustion at natural infiltration is possible, combustion at forced infiltration is expected.

Mg and Li Powders

Spherical Mg particles

- d_{50} = 32 µm (Mg30)
- d_{50} = 57 µm (Mg60)
- d_{50} = 282 µm (Mg300)

Mg flakes

- d_{50} = 28 µm

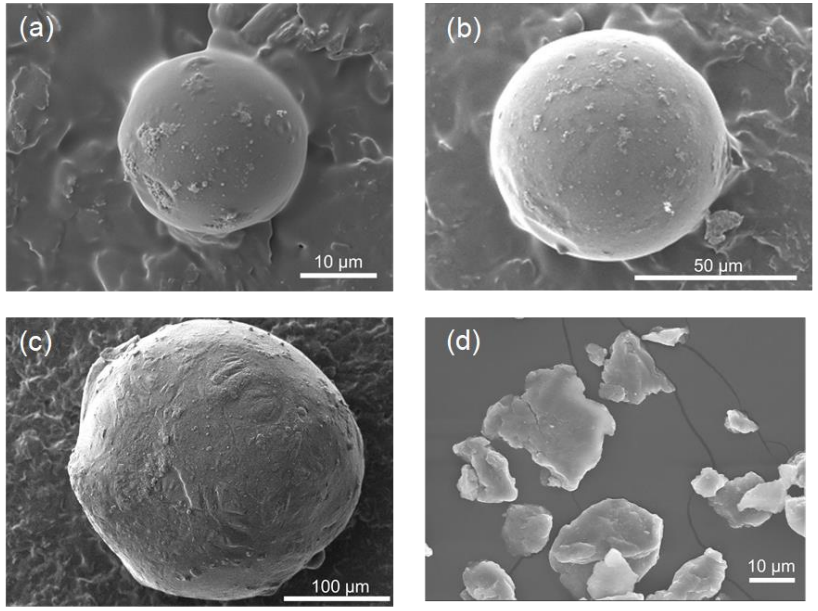

SEM images of Mg particles

Stabilized lithium metal powder (SLMP®)

- Non-pyrophoric in dry air due to Li_2CO_3 coating.
- d_{50} = 50 µm

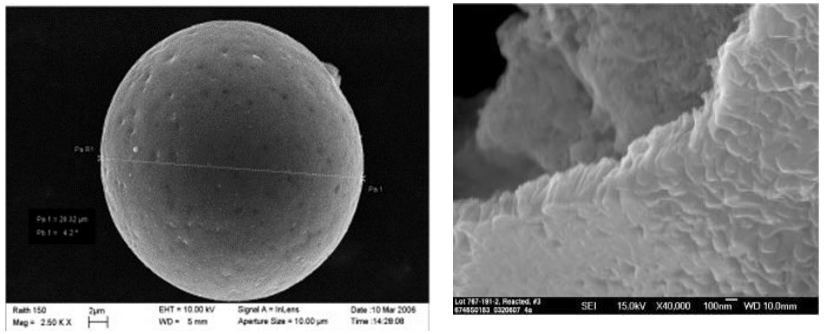

SEM images of an SLMP particle and a broken edge of the coating on a reacted SLMP particle

S. Cordova et al., "Oxidation kinetics of magnesium particles determined by isothermal and non-isothermal methods of thermogravimetric analysis," *Combustion and Flame* 238 (2022) 111950

Y. Li and B. Fitch, "Effective enhancement of lithium-ion battery performance using SLMP," *Electrochemical Communications* 13 (2011) 664

Thermoanalytical Studies

- **Thermogravimetric analysis (TGA) and differential scanning calorimetry (DSC)**
  - Sample: 0.5-1.0 mg
  - Gas environments: O_2, O_2/Ar, CO_2
  - Non-isothermal tests
    - Heating rates: 1 – 10 K/min
  - Isothermal tests
    - Temperatures: 300 – 575 °C
- **Scanning electron microscopy (SEM)**
- **X-ray diffraction analysis (XRD)**

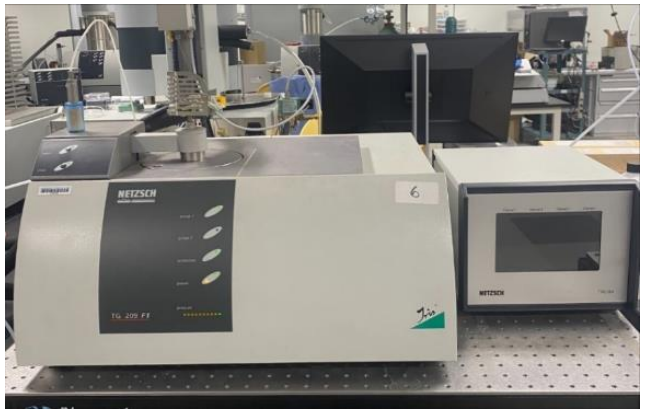

Netzsch TG 209 F1 Iris

Netzsch DSC 404 F1 Pegasus

Non-isothermal TGA of Mg in O_2

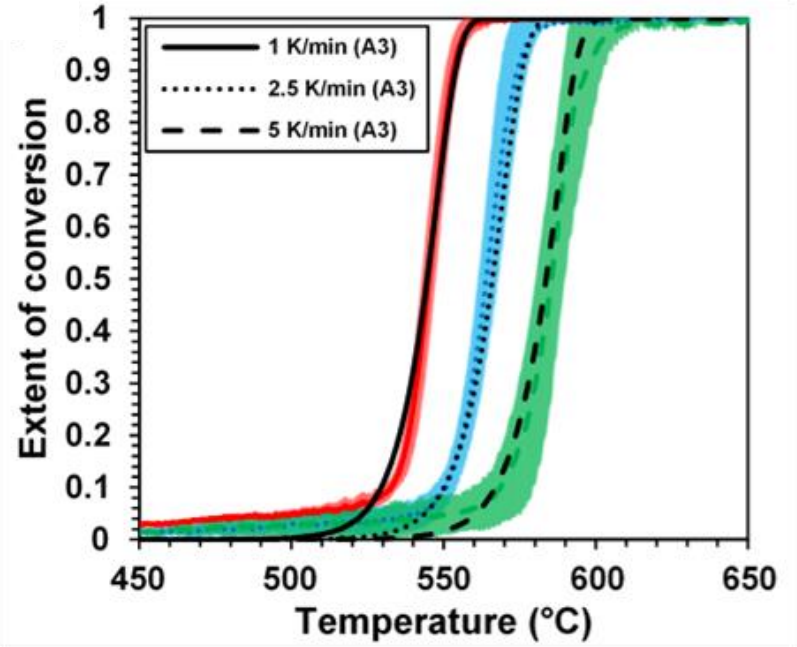

TGA curves for Mg30 fitted to the Avrami-Erofeev model

- Oxidation is complete before melting of Mg (650 °C).
- The Avrami-Erofeev model (both nucleation and growth occur in the bulk) provides the best fit with the TGA curves.

$$\frac{d\alpha}{dt} = A \exp\left(-\frac{E}{RT}\right) f(\alpha)$$

$$f(\alpha) = n(1-\alpha)[-ln(1-\alpha)]^{(n-1)/n}$$

- Apparent activation energy: 200 – 230 kJ/mol
- Submicron grains are consistent with the Avrami-Erofeev model.

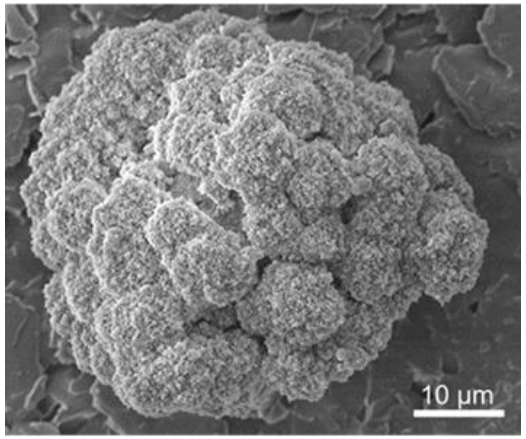

SEM image of Mg30 particle after oxidation

S. Cordova et al., "Oxidation kinetics of magnesium particles determined by isothermal and non-isothermal methods of thermogravimetric analysis," *Combustion and Flame* 238 (2022) 111950

Isothermal TGA of Mg in O_2

$$f(\alpha) = n(1-\alpha)[-ln(1-\alpha)]^{(n-1)/n}$$

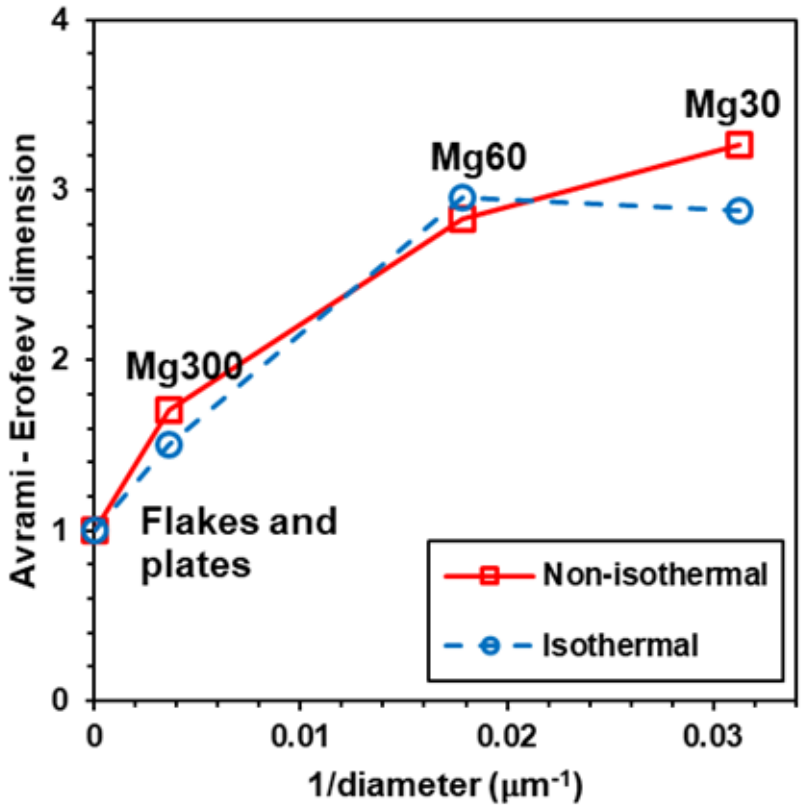

The dimension *n* of the Avrami-Erofeev equation vs. the reciprocal of the diameter

- The dimension *n* of the Avrami-Erofeev equation decreases with decreasing the curvature.

Mampel-Delmon analysis of the isothermal TGA data

- Nucleation on the surface and isotropic growth inward.
- Small (30 – 60 μm) spherical particles: slow nucleation.
  - ***n* = 3**
- With increasing size (300 μm), nucleation is faster, and its effect on the overall kinetics is smaller.
  - ***n* < 2**
- Flakes and plates: The overall kinetics is determined by the growth of a non-protective oxide layer.
  - ***n* = 1** $f(\alpha) = 1-\alpha$ – linear oxidation law

S. Cordova et al., "Oxidation kinetics of magnesium particles determined by isothermal and non-isothermal methods of thermogravimetric analysis," *Combustion and Flame* 238 (2022) 111950

Non-isothermal TGA of Mg in CO_2

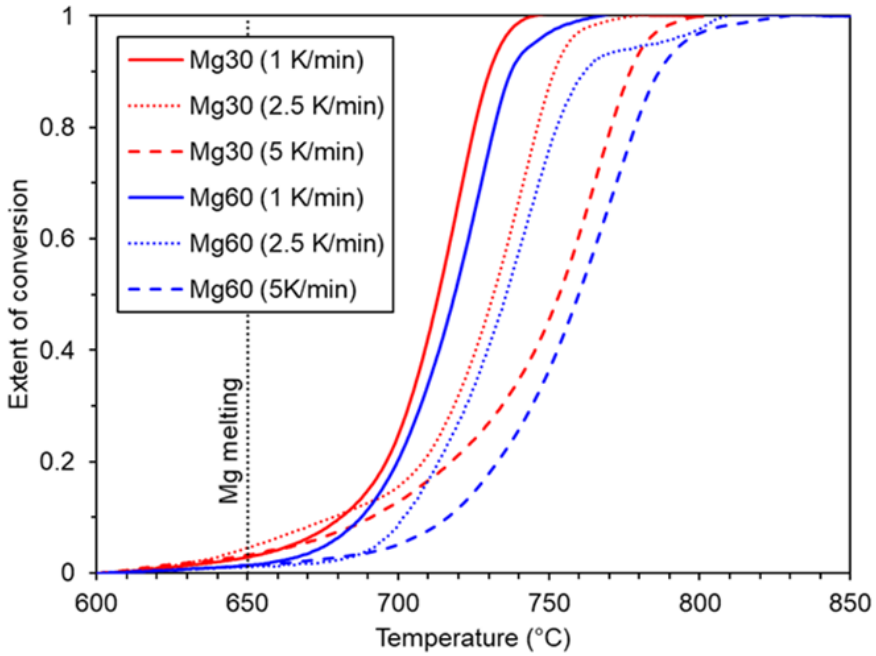

TGA of Mg particles in CO_2

- Significant conversion only after melting

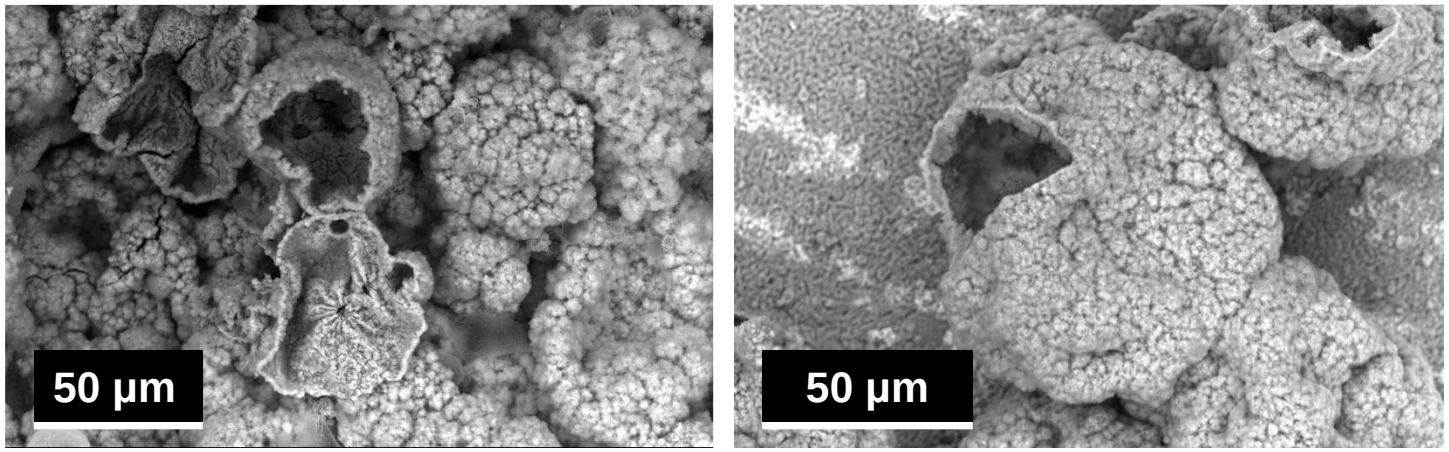

SEM images of Mg30 (left) and Mg60 (right) particles after reaction with CO_2

- **Hollow spheres:** Molten Mg spreads outward through the pores and reacts with CO_2 on the outer surface.

S. Cordova et al., "Oxidation and combustion of lithium and magnesium powders for space power applications," *International Journal of Energetic Materials and Chemical Propulsion* 22(6) (2023) 53-66.

Non-isothermal TGA of Li in O_2/Ar

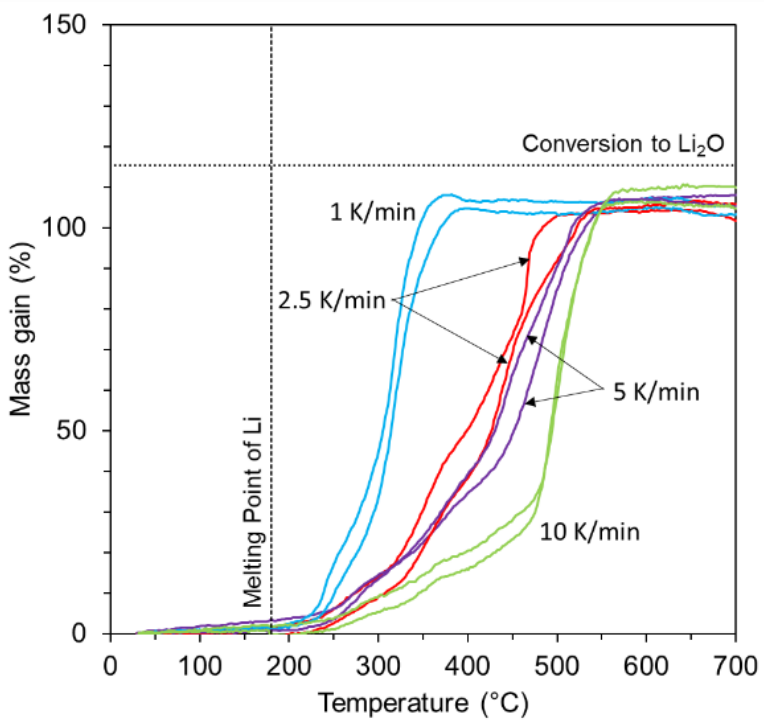

TGA of Li particles in O_2/Ar (10% O_2)

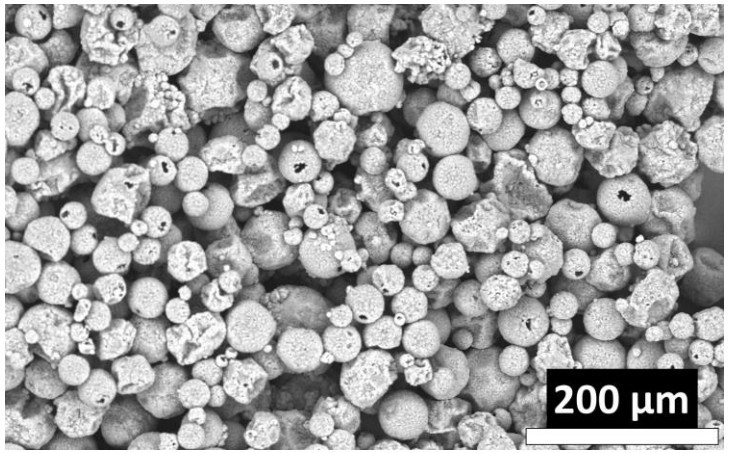

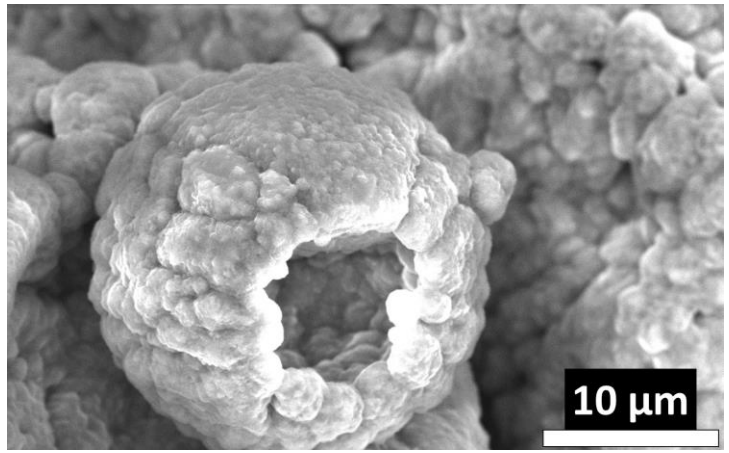

SEM images of Li particles after oxidation

- **Hollow spheres:** Molten Li spreads outward through the pores and reacts with O_2 on the outer surface.

- Mass gain is close to 115% – oxidation of Li to Li_2O.
- Reaction occurs after melting of Li.
- Transition to a faster second stage

K. Estala-Rodriguez et al., "Oxidation and combustion of stabilized lithium metal powder (SLMP)," *Proceedings of the Combustion Institute* 39 (2023) 3583-3592

Isothermal Oxidation of Li in O_2/Ar

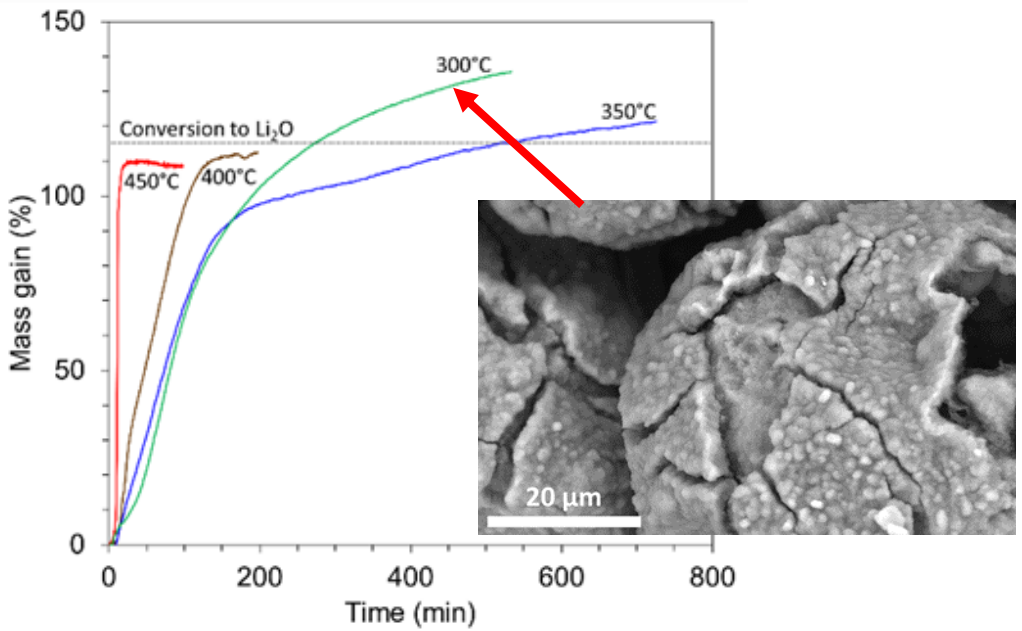

TGA of Li particles in O_2/Ar (10% O_2)

- At 300 and 350 °C, the mass gain indicates formation of Li_2O_2 along with Li_2O.
- At 400 and 450 °C, only Li_2O forms.
  - Li_2O_2 decomposes.

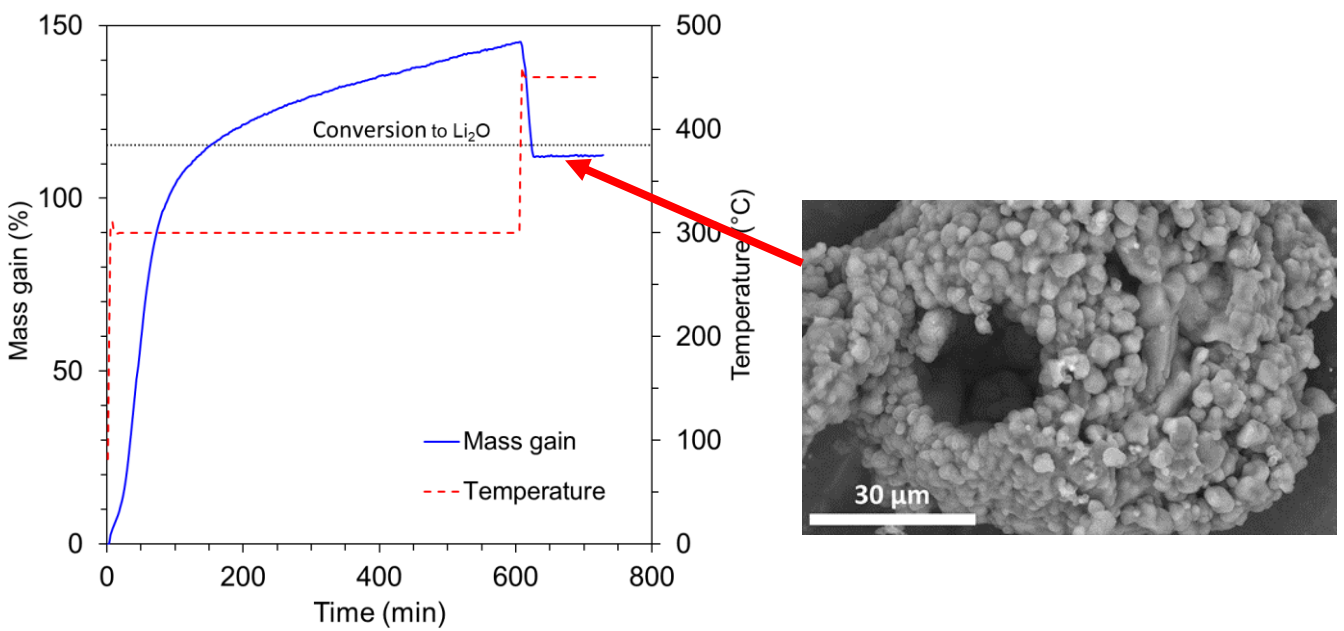

- Test to confirm formation and decomposition of Li_2O_2
  - After 600 min of heating at 300 °C, the temperature was raised to 450 °C.
  - The mass dropped to about 115%.
- **Decomposition of Li_2O_2 explains the transition to a faster reaction in the non-isothermal TGA tests.**

K. Estala-Rodriguez et al., "Oxidation and combustion of stabilized lithium metal powder (SLMP)," *Proceedings of the Combustion Institute* 39 (2023) 3583-3592

Non-isothermal TGA of Li in CO_2

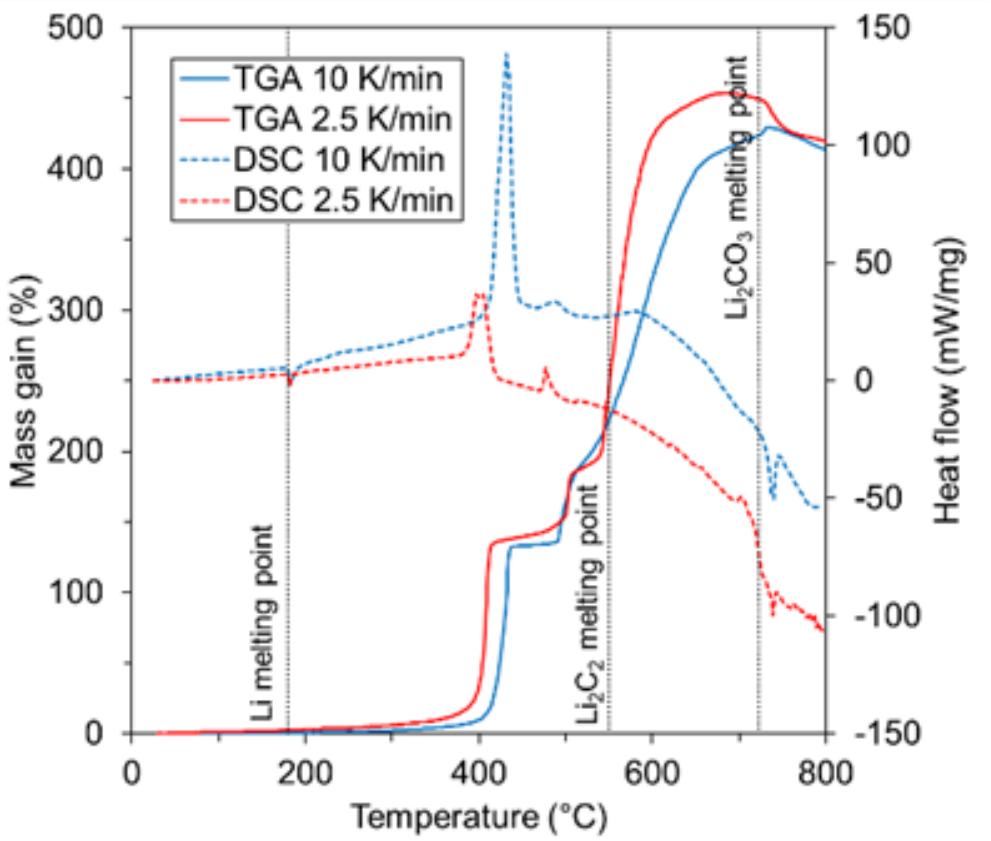

TGA and DSC of Li particles in CO_2

- Reaction starts after melting of Li.

1. **Formation of Li_2O**
   - At about 400 °C
   - $2Li + CO_2 \rightarrow Li_2O + CO$
   - $4Li + CO_2 \rightarrow 2Li_2O + C$

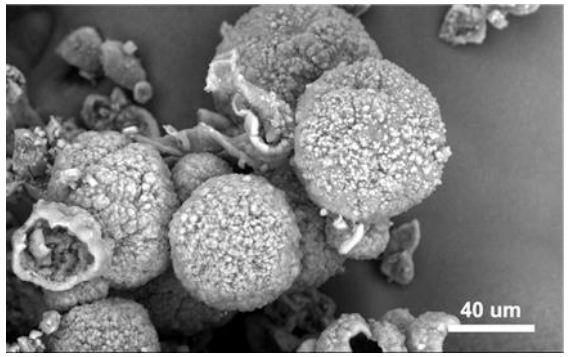

2. **Formation of Li_2CO_3**
   - At 500 – 700 °C
   - $Li_2O + CO_2 \rightarrow Li_2CO_3$

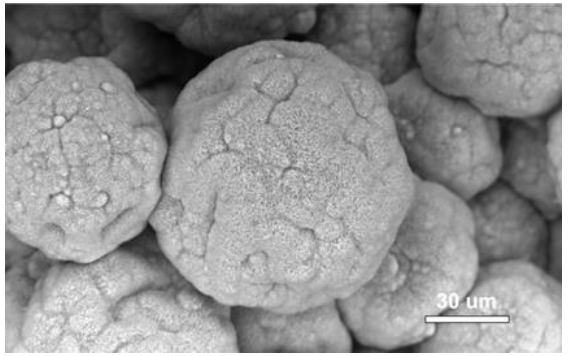

3. **Melting and decomposition of Li_2CO_3**

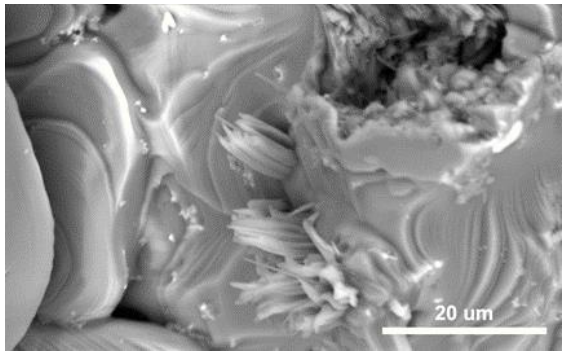

K. Estala-Rodriguez et al., "Oxidation and combustion of stabilized lithium metal powder (SLMP)," *Proceedings of the Combustion Institute* 39 (2023) 3583-3592

Combustion Experiments

- **Windowed vacuum chamber**
- **Metal powder in a quartz tube**
  - ID: 2-7 mm
  - Gas infiltrates from both ends.
- **Environments: O_2 and CO_2**
  - Pressure: 13 – 90 kPa
- **Laser ignition at the top**
- **Diagnostics**
  - High-speed video recording
  - Infrared video recording
  - Thermocouple measurements
  - Analysis of products

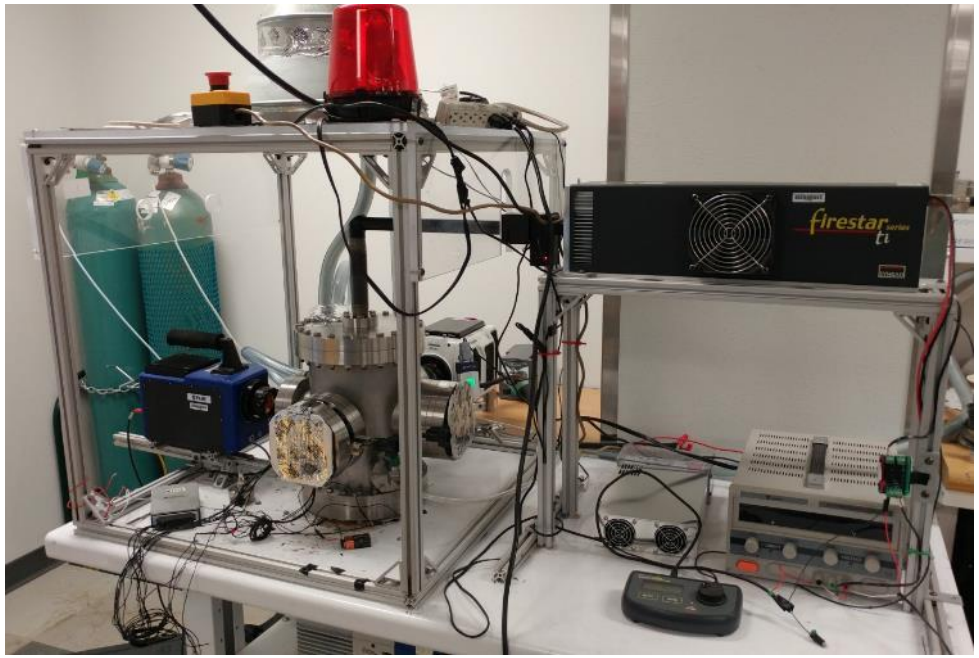

Laser ignition setup

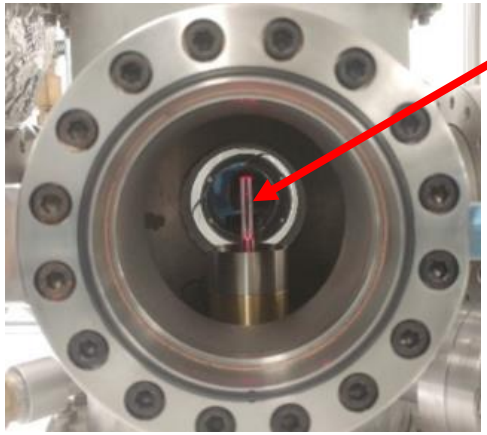

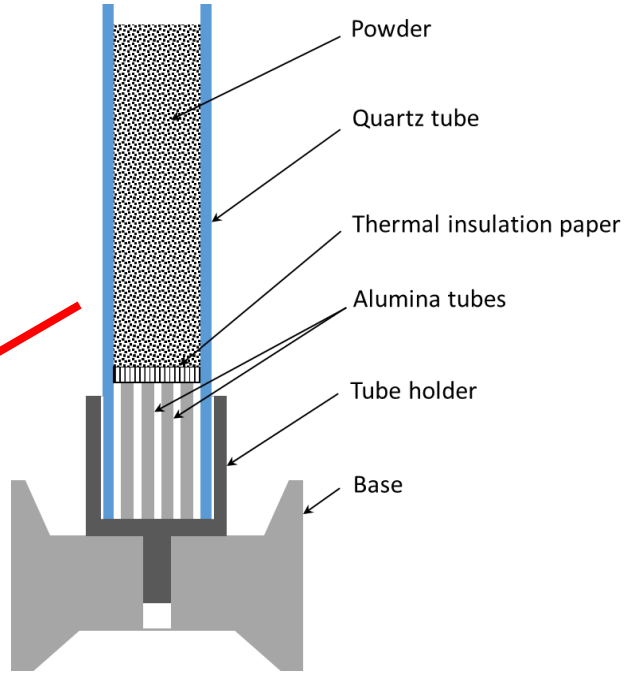

Quartz tube with sample

Combustion of Mg Powder in O_2

***ID* = 7 mm, *P* = 90 kPa**

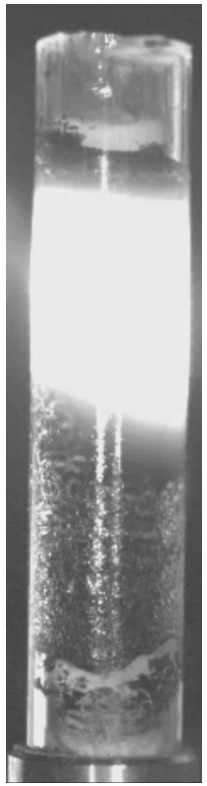

Video plays at 5x speed

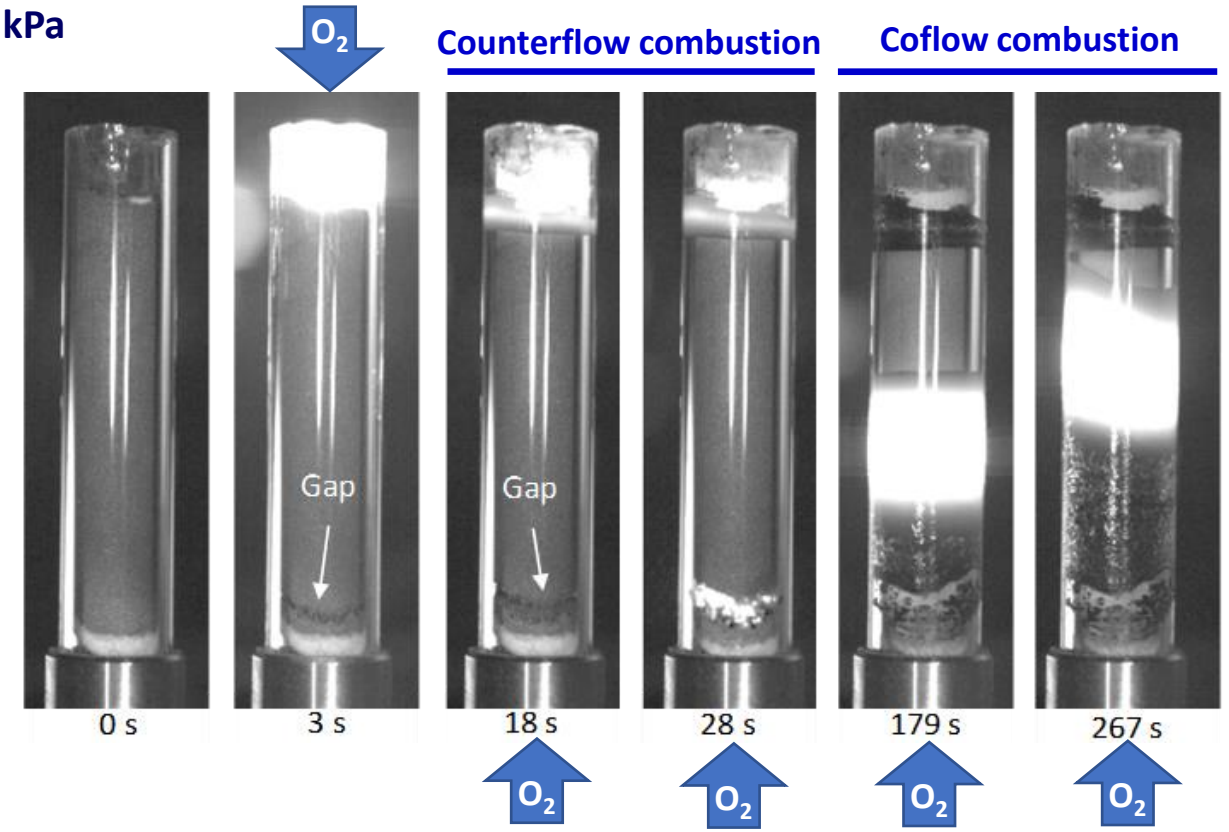

1. Ignition at the top, formation of a gap at the bottom
2. Downward propagation of a counterflow combustion wave
3. Upward propagation of a coflow combustion wave

Wave down

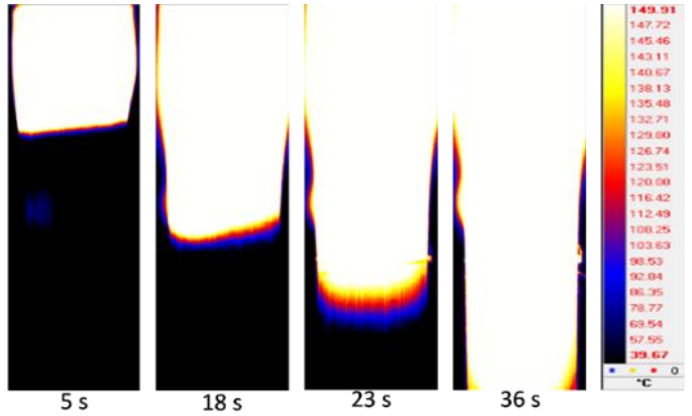

Wave up

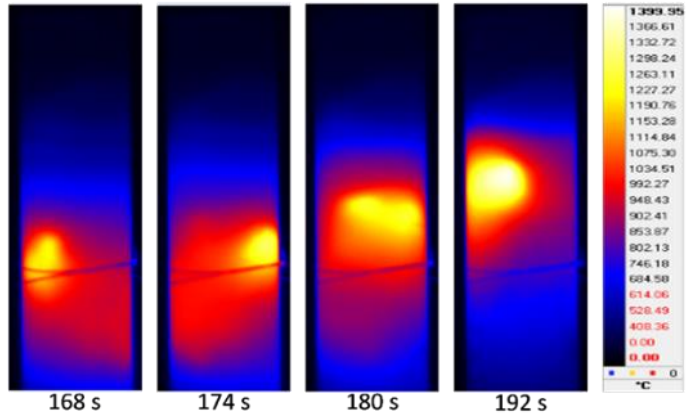

Infrared video recording

S. Cordova et al., "Infiltration-controlled combustion of magnesium for power generation in space," *Combustion and Flame* 238 (2022) 111950

Combustion of Mg Powder in O_2, Cnt'd

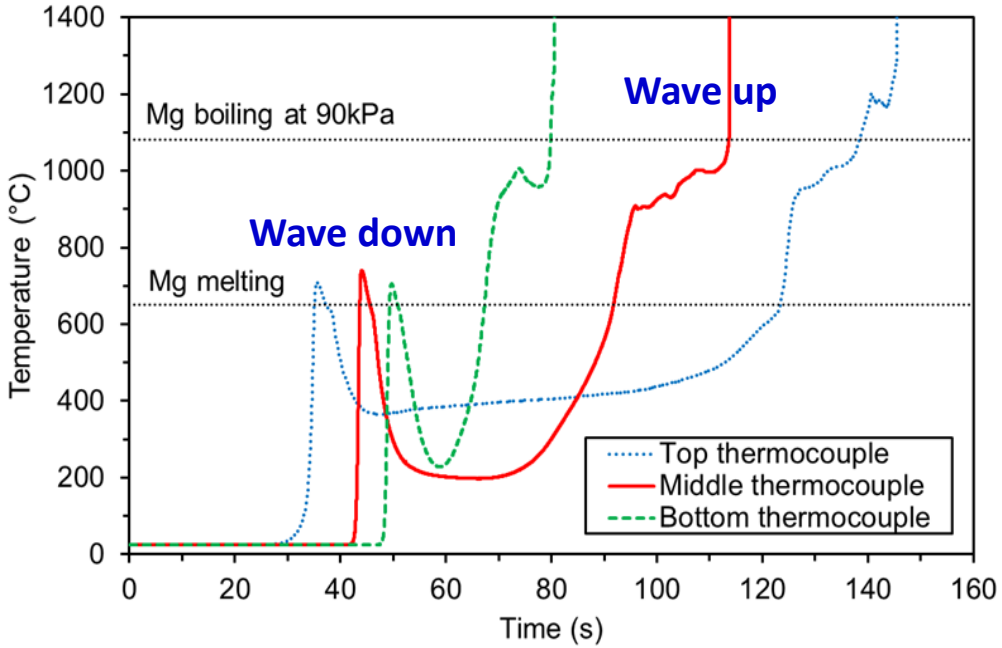

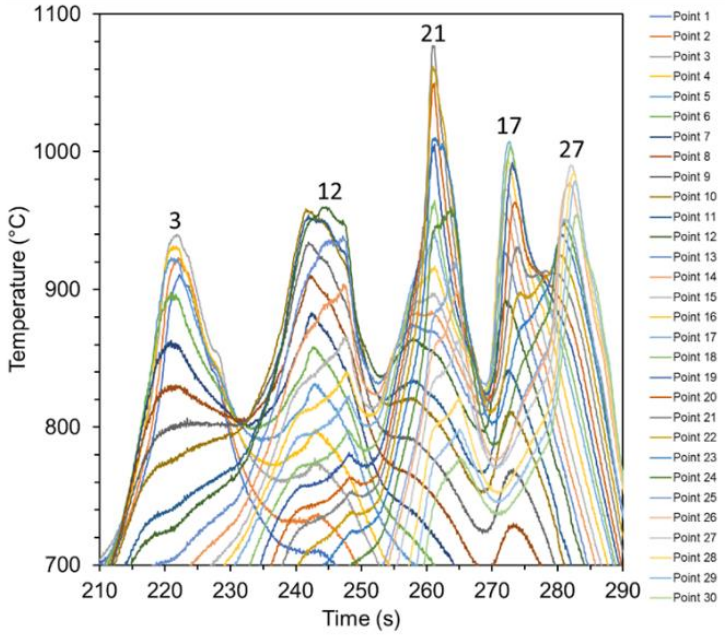

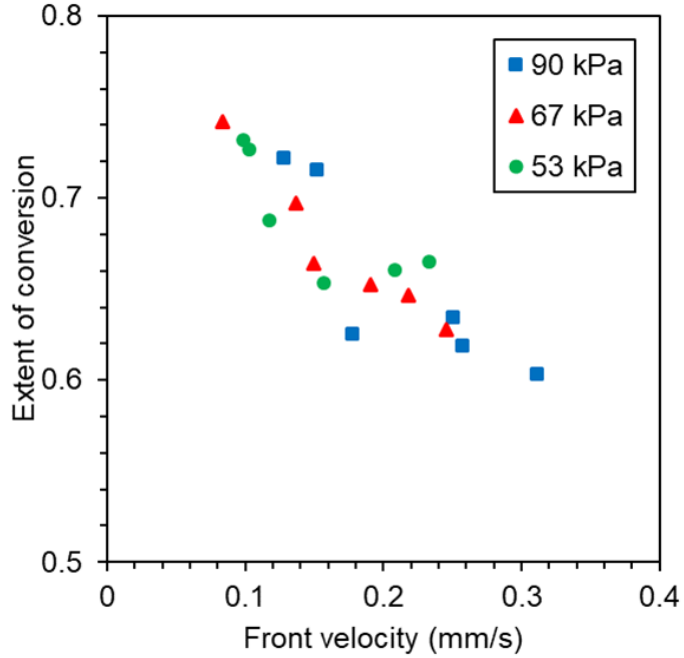

Thermocouple measurements confirm two combustion waves

1. Wave down
2. Wave up

Analysis of infrared video images for the upward wave

- Spinning propagation

- Lower front velocity increases conversion.
- Front velocity: 0.1 – 0.3 mm/s

S. Cordova et al., "Infiltration-controlled combustion of magnesium for power generation in space," *Combustion and Flame* 238 (2022) 111950

Combustion of Li Powder in O_2

***ID* = 4 mm, *P* = 90 kPa**

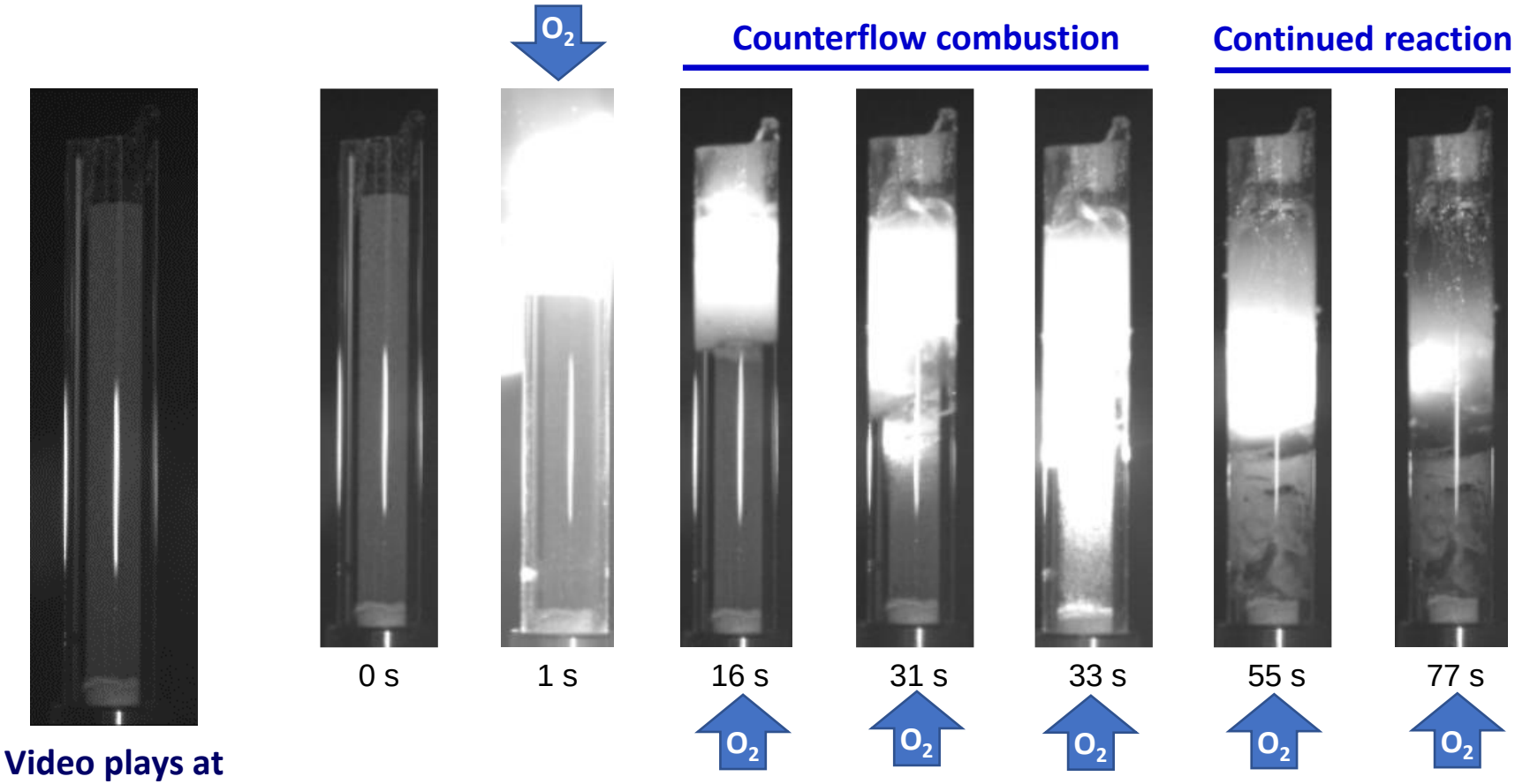

Video plays at actual speed

1. Ignition forms an impermeable product layer.
2. A thermal wave propagates downward (0.2 – 0.3 mm/s), while oxygen infiltrates from the bottom.
3. Reaction continues over the entire sample.

K. Estala-Rodriguez et al., "Oxidation and combustion of stabilized lithium metal powder (SLMP)," *Proceedings of the Combustion Institute* 39 (2023) 3583-3592

Combustion of Mg and Li Powders in CO_2

Self-sustained propagation of the combustion wave was not achieved in CO_2.

Transport of CO_2 could be hindered by:

- A protective product layer (MgO/C and Li_2CO_3/C) on the particle surface
- CO in the pores between the particles

$2Mg + CO_2 \rightarrow 2MgO + C$	R_{PB} = 1.02 – protective
$Mg + CO_2 \rightarrow MgO + CO$	R_{PB} = 0.81 – non-protective, CO forms
$4Li + 3CO_2 \rightarrow 2Li_2CO_3 + C$	R_{PB} = 1.45 – protective
$2Li + 2CO_2 \rightarrow Li_2CO_3 + CO$	R_{PB} = 1.35 – protective, CO forms

Conclusions

Conceptual design of a power system based on combustion of metal powders

- The use of Li and Mg fuels with chemical oxygen generators for heat and power production during lunar night is competitive with Li-SF_6 combustion.

High-temperature oxidation of Mg and Li powders

- Oxidation of Mg particles in O_2 is well described by the Avrami-Erofeev equation, while the Mampel-Delmon analysis shows how that the dependency of the model parameters on the particle size is related to the rates of nucleation and growth.
- Oxidation of Li particles by O_2 involves formation and then decomposition of Li_2O_2.
- Reaction of Li with CO_2 first produces Li_2O, which is then converted into Li_2CO_3.

Combustion of Mg and Li powders with infiltrating oxygen

- Ignition results in a counterflow combustion wave at incomplete conversion, followed by a backward coflow wave or by a reaction over the entire sample.

Thank you!